Structural Plasticity of Peptidyl−Prolyl Isomerase sFkpA Is a Key to Its Chaperone Function As Revealed by Solution NMR†

Kaifeng Hu,*,‡ Veniamin Galius,§ and Konstantin Pervushin*

Laboratorium für Physikalische Chemie, ETH-Zürich, Wolfgang-Pauli-Strasse 10, CH-8093 Zürich, Switzerland

Received April 23, 2006; Revised Manuscript Received July 27, 2006

ABSTRACT: Intramolecular dynamics of periplasmic chaperone FkpA-ΔCT (sFkpA) and its complexes with partially structured substrates are studied by NMR in solution. The backbone amide ^{15}N relaxation of sFkpA reveals flexibility in the relative orientation between the dimerization domain and two juxtaposed catalytic domains identified in the X-ray structure of sFkpA. This flexibility is attributed to the structural plasticity within the long α-helical arm (helix III) consisting of residues 84 and 91. Residual dipolar couplings (RDCs) indicate an absence of fixed orientation between the sFkpA domains. The substrate binding surface of sFkpA is defined on the X-ray structure by mapping of chemical shift perturbations introduced by complexation of sFkpA with its corresponding protein substrates: partially folded RNase A S-protein and reduced carboxymethylated bovine α-lactalbumin (RCM-la). A comparison of ^{15}N relaxation of apo-sFkpA and its complex with RNase A S-protein indicates an increased rigidity within the long α-helix III and decreased interdomain mobility of the complex. We speculate that these dynamic properties may play a key role in the chaperone activity of sFkpA, since ability to bind different substrates potentially requires structural adaptations of the chaperone protein. We show that binding of sFkpA to RNase A S-protein greatly reduces the population of aggregated oligomeric species of RNase A S-protein. Finally, a molecular model, the so-called "mother's arms" model, is proposed to illustrate the mechanism of chaperone activity by FkpA.

FkpA is a heat shock periplasmic peptidyl−prolyl *cis*/*trans* isomerase (PPIase)[1] with chaperone activity. FkpA was originally discovered as a periplasmic *Escherichia coli* homologue of the Macrophage Infectivity Potentiator (MIP) protein-like FK506-binding proteins (*1*). The mature dimeric FkpA protein has 245 residues per monomer. The recently reported crystal structure of dimeric FkpA-ΔCT indicates that FkpA is comprised of two domains per monomer, the N-terminal dimerization domain and the C-terminal FK506-binding protein (FKBP) domain. The N-terminal domain of FkpA includes three helices that are interlaced with those of the other subunit to provide all the intersubunit contacts maintaining the dimeric species. The overall form of the dimer is V-shaped. A comparison of the crystal structures of FkpA alone and in a complex with FK506 reveals flexibility in the relative orientation of the two C-terminal domains located at the extremities of the V (*2*). In solution, FkpA apparently retains a dimeric organization as is evidenced by analytical gel filtration (*3*, *4*) and by ultracentrifugation experiments (*5*).

Overexpression of FkpA suppresses the formation of inclusion bodies from a defective folding variant of the maltose-binding protein and promotes the reactivation of denatured citrate synthase (*5*). Coexpression of FkpA can dramatically improve functional periplasmic production of single-chain fragments (scFv) of antibodies, even those not containing *cis*-prolines (*6*). The yield of soluble and functional scFv fragment was also increased in vitro in the presence of stoichiometric amounts of FkpA. Recently, it was reported that covalent fusion with FkpA can increase functional solubilization of aggregation-prone HIV envelope proteins (*7*) and that the catalytic parameters for hydrolysis of ampicillin by scFv9G4H9 are clearly influenced by the presence of FkpA (*8*). The folding-assisting function of FkpA was previously hypothesized to be due to its interaction with early folding intermediates preventing their aggregation, and its ability to reactivate inactive proteins, possibly by binding to partially unfolded species (*3*). However, the molecular mechanism of the chaperone activity of FkpA remains poorly defined. There is still different opinions with regard to where the chaperone function resides in the dimeric molecule, although different reports agree that the chaperone activity of FkpA is independent of its PPIase activity (*2*, *4*).

† This work was funded by the Swiss National Foundation and the ETH Zürich.

* Corresponding authors. Prof. Konstantin Pervushin: Department of Chemistry and Applied Bioscience, Swiss Federal Institute of Technology, ETH Hönggerberg, CH-8093 Zürich, Switzerland. Phone: +41-1-632-0922. Fax: +41-1-632-1021. E-mail: kope@phys.chem.ethz.ch. Dr. Kaifeng Hu: Laboratory of Chemical Physics, NIDDK, NIH, Bethesda, Maryland 20892-0520. Phone: +1-301-451-6643. Fax: +1-301-496-0825. E-mail: hukaifeng@niddk.nih.gov.

‡ Current address: Laboratory of Chemical Physics, National Institute of Diabetes and Digestive and Kidney Diseases, National Institutes of Health, Bethesda, Maryland 20892-0520.

§ Current address: Institute of Molecular Biology and Biophysics, ETH Hönggerberg, CH-8093 Zürich, Switzerland.

[1] Abbreviations: FKBP, FK506-binding protein; PPIase, peptidyl−prolyl *cis*/*trans* isomerase; RCM-1a, reduced and carboxymethylated bovine α-lactalbumin; IPTG, isopropylthiogalactosidase; DSS, 2,2-dimethyl-2-silapentane-5-sulfonate, sodium salt; NMR, nuclear magnetic resonance; NOE, nuclear Overhauser effect; RDC, residual dipolar coupling; TROSY, transverse relaxation optimized spectroscopy; PAS, principal axis system.

10.1021/bi0607913 CCC: $33.50
Published on Web 09/12/2006

Earlier, we reported the backbone resonance assignment of 94% of the residues of FKpA and established the secondary structure elements by solution NMR (*9*). We found that overall in solution the secondary structure of the chaperone is in good agreement with the reported crystal structure (*2*) except that in solution we observe a break in the long α-helical arm (helix III) between residues 84 and 91, which may undergo conformational fluctuation on NMR signal unfavorable time scale. We hypothesized that this dynamic conformational disorder may play an important role in the chaperone activity of sFkpA, since ability to bind to different protein substrates potentially requires some structural adaptations of the chaperone. In the present work, we characterize the dynamic properties of FkpA, its interactions with polypeptide (protein) substrates such as S-protein and reduced carboxymethylated bovine α-lactalbumin (RCM-la) serving as a paradigm for destabilized and only partially folded proteins, and thereby elucidate the molecular mechanisms of sFkpA chaperone activity.

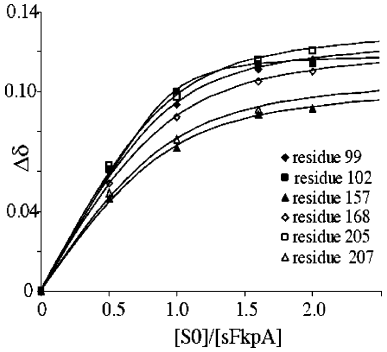

FIGURE 1: Nonlinear fit of residue-specific chemical shift changes $\Delta\delta$ of Asn 99 (◆), Lys^+ 102 (■), Asp^- 157 (▲), Phe 168 (◇), Val 205 (□), and Gly 207 (△) of sFkpA versus added substrate RNase A S-protein. K_a values and corresponding $\Delta\delta_{max}$ obtained are: K_a, 23.830, 88.777, 16.532, 17.322, 24.127, 16.061 mM^{-1} and $\Delta\delta_{max}$, 0.132, 0.120, 0.110, 0.131, 0.138, 0.116 ppm for residues 99, 102, 157, 168, 205, and 207, respectively. The solid lines represent the calculated curves with the obtained values of K_a and $\Delta\delta_{max}$ for each residue, respectively.

MATERIALS AND METHODS

Materials and Sample Preparation. Backbone ^{15}N-relaxation, ^{1}H-^{15}N residual dipolar couplings, and chaperone/substrate complex formation are studied with ^{2}H, ^{15}N-labeled sFkpA-His_6, where the functionally dispensable 9 N-terminal and 18 C-terminal amino acid residues of the mature FkpA are removed (*4*). The labeled sFkpA-His_6 (residues 10−224) with attached six histidine tag at its C-terminus was produced according to protocols described previously (*9*). The final ^{2}H, ^{15}N-labeled NMR sample of the sFkpA protein was 0.8 mM per monomer in 20 mM Mes buffer at pH 6.0 with 50 mM NaCl and 10% D_2O. Residual dipolar couplings (RDCs) for ^{1}H-^{15}N amide groups of ^{2}H, ^{15}N-labeled sFpA were measured by addition of either Pf1 filamentous bacteriophages aligned in the magnetic field or a dilute liquid crystalline phase composed of $C_{12}E_5$/hexanol/H_2O (*10*). In the former case, the sample with the aligned protein was obtained by titration of the Pf1 phages using a 50 mg/mL stock solution until the observed quadrupolar deuterium resonance splitting of the solvent signal was about 4.4 Hz (Figure S.1 B, Supporting Information). For the $C_{12}E_5$/*n*-hexanol/H_2O system forming an Lα phase in solution, 15% concentrated liquid crystals composed of $C_{12}E_5$/*n*-hexanol in 90% H_2O/10% D_2O were first prepared under vigorous shaking followed by addition of the protein sample under further vigorous shaking to form a final concentration (around 4%) suitable for RDC measurements. In some cases, addition of the protein led to phase separation, whereupon more *n*-hexanol was added to re-establish the liquid crystals (*10*).

RNase A S-protein and reduced and carboxymethylated bovine α-lactalbumin (RCM-la) were chosen as protein substrates. RNase A S-protein and carboxymethylated bovine α-lactalbumin were purchased form Sigma (lot no. L5888). The latter was reduced with dithiothreitol (DTT, also from Sigma) to generate RCM-la before titration.

NMR Experiments. NMR experiments were performed at 37 °C on a Bruker AVANCE 600 MHz spectrometer equipped with a cryogenic probe and an AVANCE 900 MHz spectrometer. NMR data were analyzed using XEASY (*11*) and CARA (www.nmr.ch) (*12*). The ^{1}H chemical shifts were referenced to the DSS (sodium 2, 2-dimethyl-2-silapentane-5-sulfonate) signal at 0 ppm, and ^{15}N chemical shifts were referenced indirectly using the $^{15}N/^{1}H$ gyromagnetic ratios (*13*).

sFkpA Backbone ^{15}N Relaxation Measurements. TROSY-based pulse sequences were used to record ^{15}N R_1 and R_2 times as well as steady-state ^{1}H-^{15}N NOEs. The ^{15}N R_1 and R_2 experiments were recorded at 37 °C at 600 MHz with 32 scans, while 64 scans were used to record the ^{1}H-^{15}N NOE experiments. The ^{15}N R_1 times were measured using spectra recorded with 10 different durations of the relaxation delays of 20, 90, 160, 200, 300, 400, 600, 800, 1000, and 1200 ms. The R_2 values were determined from spectra recorded with delays 2, 8, 12, 24, 30, 35, 40, 50, 70, and 90 ms. In order to eliminate the effects of cross-correlation between ^{1}H-^{15}N dipolar and ^{15}N CSA relaxation mechanisms, the ^{1}H spins were continuously decoupled during entire relaxation delay. The ^{1}H-^{15}N steady-state NOE rates were obtained from NOE and reference spectra recorded in the presence and absence of a proton saturation period of 3 s. In the case of the reference spectra, a net relaxation delay of 5 s was employed, while a relaxation delay of 2 s prior to a 3 s proton saturation period was employed for the NOE spectra. For backbone R_1 and R_2 values measurements of sFkpA in complex with S-protein, the ^{2}H, ^{15}N-labeled sFkpA was mixed with S-protein at a molar ratio about 1:4. Under these conditions, sFkpA was assumed to be saturated with S-protein and exist mostly in the complexed form. The R_1 and R_2 rates were determined by fitting the measured peak heights to a single-exponential two-parameter decay function (*14*). Error analysis was performed assuming that the noise level measured in the spectrum at the first relaxation time point had the same level in the remaining nine spectra recorded at different relaxation delays. The measured cross-peak intensities were randomly varied within the range of estimated noise amplitude to generate 100 sets of relaxation data. Fitting was then carried out for these 100 sets of data resulting in 100 R_1 and R_2 values, which are used to estimate the statistical variations in the reported R_1 and R_2 rates (Figure 3).

Mesurement of ^{1}H-^{15}N Residual Dipolar Couplings of sFkpA. Magnetic alignment of the Pf1 phage was monitored by observation of the ^{2}H quadrupolar splitting in a 1D ^{2}H NMR spectrum of the solvent as a function of the phage

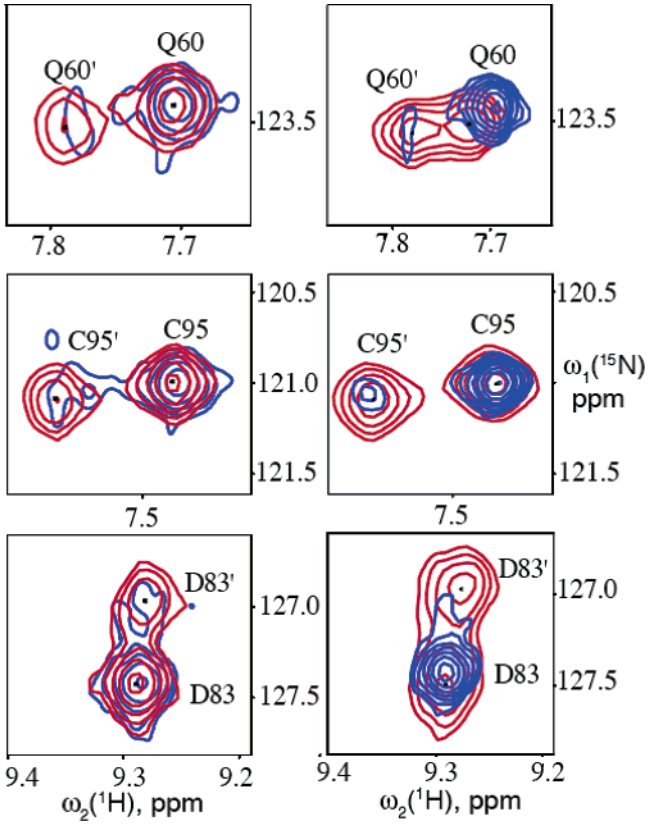

FIGURE 2: Expansions of a [^{1}H,^{15}N]-TROSY-HSQC spectrum of 0.156 mM S-protein (red) are overlaid with corresponding expansions of a spectrum of 0.156 mM S-protein in the presence of equally concentrated sFkpA measured at 25 °C (blue) (left panel). The same regions from a [^{1}H,^{15}N]-TROSY-HSQC spectrum of S-protein at 1.06 mM concentration (red) are overlaid with a spectrum of S-protein diluted by buffer to 0.08 mM concentration (blue) (right panel). The expansions show three different backbone amide resonances of RNase A S-protein for which both signals arising from the monomer and the dimer states of RNase A S-protein are observable (Q60, D83, and C95). The cross-peaks marked by primed labels correspond to the oligomers of RNase A S-protein and are reduced in amplitude relative to the monomer peaks upon dilution of RNase A S-protein. The blue and the red spectra are normalized to show the same number of contours for the monomer peaks. The dimer peaks are 3−4 times reduced in intensity in presence of sFkpA chaperone as compared to the corresponding monomer peaks.

concentration (Figure S.1 B, Supporting Information). The observed quadrupolar splitting varies approximately linearly with the phage concentration (up to 60 mg/mL of phage) (*15*). In order to extract RDCs in the ^{2}H, ^{15}N-labeled sFkpA sample, we measured the separation of multiplet components in the directly detected ^{1}H dimension (*16*). To improve resolution in the ^{15}N dimension, TROSY and ^{1}H-anti-TROSY spectra (Figure S.1 A, Supporting Information) were recorded separately using 0.8 mM ^{2}H, ^{15}N-labeled sFkpA at 37 °C at a ^{1}H frequency of 900 MHz. RDCs were obtained from ^{1}H resonance positions in TROSY and ^{1}H-anti-TROSY spectra upon addition of the Pf1 phages. TROSY and ^{1}H-anti-TROSY spectra (not shown) were also recorded using 0.8 mM ^{2}H, ^{15}N-labeled sFkpA at 25 °C and 900 MHz in the presence and absence of the liquid crystal of $C_{12}E_5$/*n*-hexanol/H_2O. Under these conditions, observed deuterium quadrupolar splitting of the solvent signal in 1D ^{2}H NMR spectrum was 18.6 Hz.

Formation of Chaperone/Substrate Complexes. Chemical shift perturbations of the ^{1}H and ^{15}N backbone resonances of sFkpA were observed during titration with either RNase A S-protein or RCM-la, respectively. S-protein is a 104 amino acid polypeptide derived from RNase A which retains some residual structure that is stabilized by four disulfide bonds (*17*, *18*). By limited proteolysis, the peptide bond between A20−S21 of RNase A is selectively cleaved, resulting in a structurally only slightly altered, but enzymatically fully active complex (*19*). By removal of the N-terminal 20 amino acid peptide, the enzymatically inactive, but folding-competent, RNase A S-protein is generated. Reduced and carboxymethylated bovine α-lactalbumin (RCM-la) is a denatured protein with molecular weight of 14 kDa and is unfolded under physiological conditions and remains water soluble under conditions of our solution NMR study (*4*). A series of 2D [^{1}H, ^{15}N]-TROSY-HSQC spectra (Figure S.2, Supporting Information) were recorded using ^{2}H/^{15}N-labeled sFkpA at 37 °C at 900 MHz before and during the process of titration at molar ratios of 1:0, 1:0.5, 1:1, 1:1.6, and 1:2 for S-protein and for RCM-la, respectively.

A 0.2 mM sample of ^{15}N-labeled RNase A S-protein in 20 mM MES buffer was titrated with a 1.45 mM stock solution of none-labeled sFkpA. A series of 2D [^{1}H,^{15}N]-TROSY-HSQC spectra were acquired at concentration ratios of 1:0, 1:0.5, 1:1, and 1:1.5 of S-protein to sFkpA at 11 and 25 °C. During this titration, the S-protein concentration decreased due to dilution from 0.2 mM to 0.175, 0.156, and 0.141 mM, respectively. A part of the same S-protein sample was diluted with 20 mM MES buffer to a concentration of 0.156 mM S-protein, and reference spectra at 11 and 25 °C were measured.

RESULTS AND DISCUSSION

Misfolded proteins pose a potential threat to the cell due to their increased tendency to aggregate. An important function of protein chaperones is to bind nonnative, misfolded, or partially folded states of expressed or translocating proteins thereby preventing their aggregation (*20*, *21*). FkpA is a ubiquitous periplasmic peptidyl−prolyl *cis/trans* isomerase shown to decrease formation of inclusion bodies and promote the reactivation of denatured states of some proteins (*5*) and thus acts as an ATPase-independent chaperone. Despite the importance of this function, surprisingly little is know about the mechanistic details of chaperone/substrate interactions. Here, we report on molecular details of binding of partially folded polypeptides to sFkpA as well as corresponding changes in intramolecular dynamics of the chaperone in a response to substrate binding. On the basis of our data, we propose a mechanistic model of the chaperoning function of FkpA.

Interactions of sFkpA with Partially Folded Polypeptides. The selection of the polypeptide substrates suitable for solution NMR studies of the chaperone function of FkpA requires that the candidate polypeptide is partially folded or misfolded or forms relatively stable intermediates on its refolding pathway, and is of a moderate molecular weight. Since FkpA prevents formation of aggregates, we sought polypeptide substrate which ideally are in a dynamic equilibrium with aggregated states and yet remained water-soluble at high concentrations. We have chosen the RNase

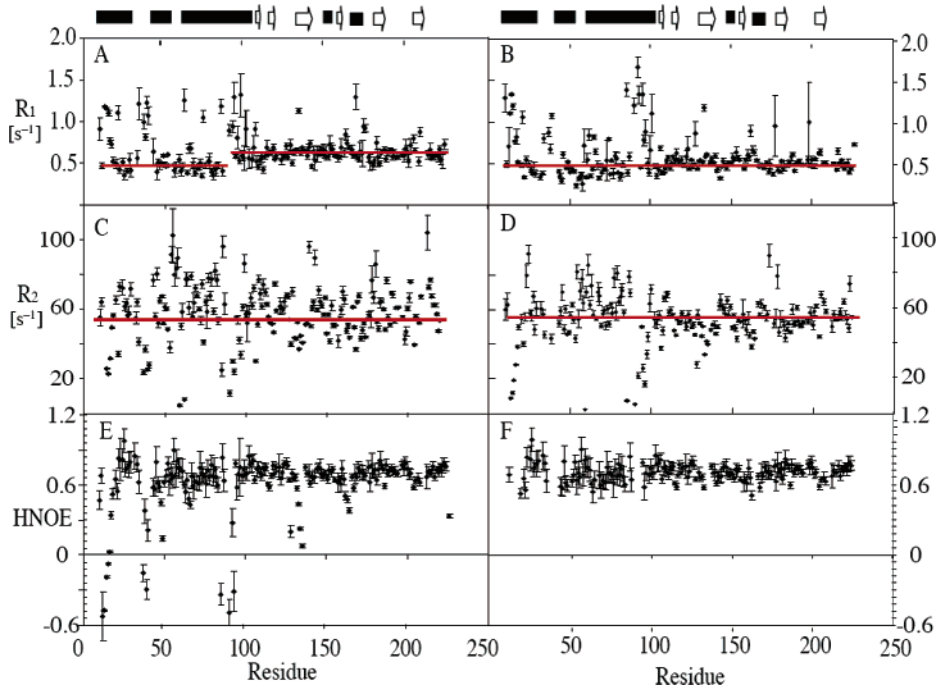

FIGURE 3: Plots of (A) R_1, (C) R_2, and (E) ^{1}H {^{15}N}-heteronuclear NOE of free sFkpA and (B) R_1, (D) R_2, and (F) ^{1}H {^{15}N}-heteronuclear NOE of sFkpA in a 1:4 complex with S-protein versus residue number. Horizontal lines represent the average relaxation rates for the residues 10−91 and 92−220, respectively. The secondary structure elements are shown on the top, in which solid lines represent α-helix and arrows are β sheets.

A S-protein and reduced and carboxymethylated bovine α-lactalbumin (RCM-la) (*3*, *4*) as partially folded protein substrates. In comparison with RCM-la, S-protein appears not only to satisfy all aforementioned conditions, but is available in ^{13}C, ^{15}N-labeled form (manuscript in preparation), so that some insight on the chaperone function can be obtained by observing the substrate.

The response of FkpA to titration of protein substrates is monitored via an index of cumulative changes in ^{1}H and ^{15}N chemical shifts (*22*). Significant perturbations in the electronic environment of reporter spins of residues Val 142, Val 143, Asp$^-$ 157, Phe 168, Arg$^+$ 169, Val 205, and Gly 207 caused by binding of both RCM-la and S-protein are observed (Figure S.2, Supporting Information). In table S.4 A and B, the residues are listed in descending order according to the calculated chemical shift changes upon addition of equimolar RNase A S-protein or RCM-la. Most of the affected residues are hydrophobic and line the inner surface of the V-shaped molecule of sFkpA (Figure 5). These residues form two spatially close groups, as shown in magenta on the right monomer in Figure 5. The first one consists of Val 205 and Gly 207, which are believed to be involved in hydrophobic interaction with inhibitors of PPIase activity (*2*). The second group includes Val 142, Val 143, Asp$^-$ 157, and Phe 168/Arg$^+$ 169 (for substrates RNase A S-protein/ RCM-la, respectively). Residues Val 142, Val 143, and Phe 168 probably form a second hydrophobic interaction patch with substrates, and Asp$^-$ 157 and Arg$^+$ 169 are likely to be involved in electrostatic interactions with some residues on the surface of the substrates. In a complex with S-protein, residues Asn 99, Lys$^+$ 102, Gly 103 and Glu$^-$ 105 show significant chemical shift changes, which are not observed in interactions with RMC-la. These residues, situated in the long α-helix arm (helix III) form another direct binding site for the substrate RNase A S-protein or as a result of a conformational change in sFkpA induced by initial binding of the substrate to the catalytic (FKBP) domains of the chaperone.

To address the residue-specific binding properties of sFkpA and S-protein quantitatively, chemical shift changes for residues Asn 99, Lys$^+$ 102, Asp$^-$ 157, Phe 168, Val 205, and Gly 207 chosen from the three groups mentioned above (Table S.4 C, Supporting Information) are used to extract the residue-specific association constants (K_a). Because only a single set of NMR signal peaks is observed for the mixture of S-protein and sFkpA, we conclude that under the conditions studied free and substrate-loaded forms of sFkpA are in fast exchange. For two site exchange, a nonlinear fit of the residue-specific chemical shift change $\Delta\delta$ at corresponding volume v of added substrate RNase A S-protein yields residue-specific K_a values as well as the corresponding $\Delta\delta_{max}$ (*23*). The obtained K_a values for residues Asp$^-$ 157, Phe 168, Val 205, and Gly 207 are close to an average value of $K_a = 18.5$ mM^{-1}, indicating that these residues are involved in a single binding event on the surface of sFkpA. When binding with S-protein, sFkpA may possess a second binding site located on the long α-helix arm (helix III) consisting of Asn 99, Lys$^+$ 102, Gly 103, and Glu$^-$ 105, or alternatively, these changes might be induced by propagating of structural perturbations from the primary binding site. The difference in binding sites of sFkpA in complex with RNase A S-protein and its complex with RCM-la observed in our NMR experiments clearly indicates the commonality of the two substrates binding sites, which can serve as an explanation of previously reported ambiguities (*2*, *4*).

One of the main functions of sFkpA might be to prevent aggregation of substrate polypeptide. Indeed, we directly observed that sFkpA prevents oligomerization of RNase A S-protein. The effect of sFkpA-chaperone on the oligomeric states of S-protein was studied using ^{15}N-labeled S-protein

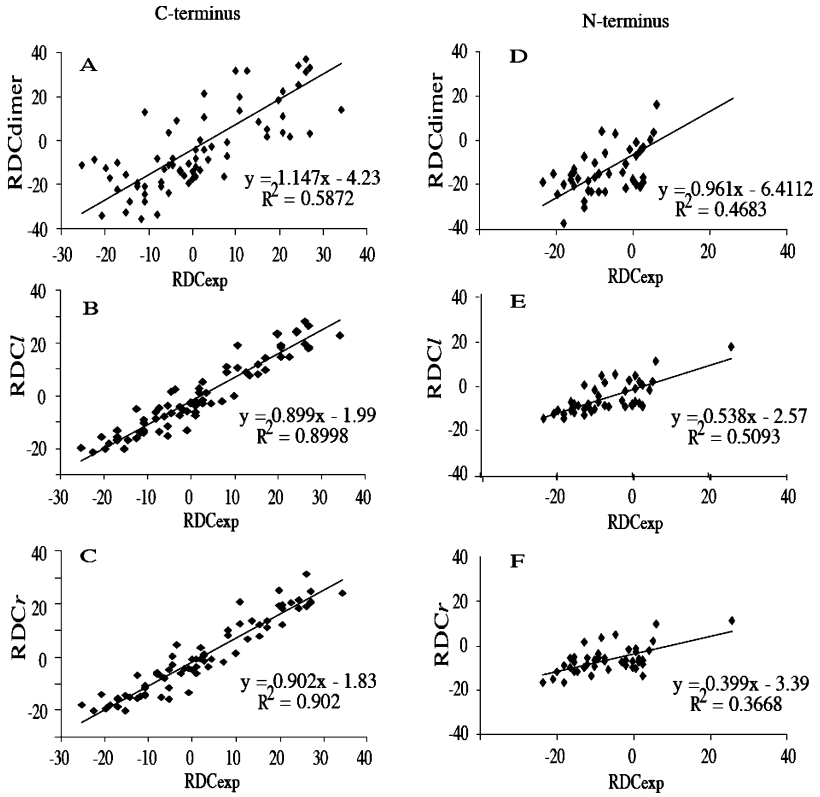

FIGURE 4: Correlation between the experimental residual dipolar couplings, RDC_{exp}, and calculated residual dipolar couplings RDC_{calc} based on different alignment tensor fitting models for the C-terminal domain (residues 116 − 224) (A−C) and N-terminal domain (residues 18−112) (D−F) of sFkpA measured in the presence of Pf1 filamentous bacteriophage. (A and D) Fitting experimental data to a single alignment tensor using a rigid dimer molecular model derived from the X-ray structure (*2*); (B and E) and (C and F) fitting experimental data using atomic coordinates of either the monomer *l* or monomer *r* from the X-ray structure as a molecular model, respectively.

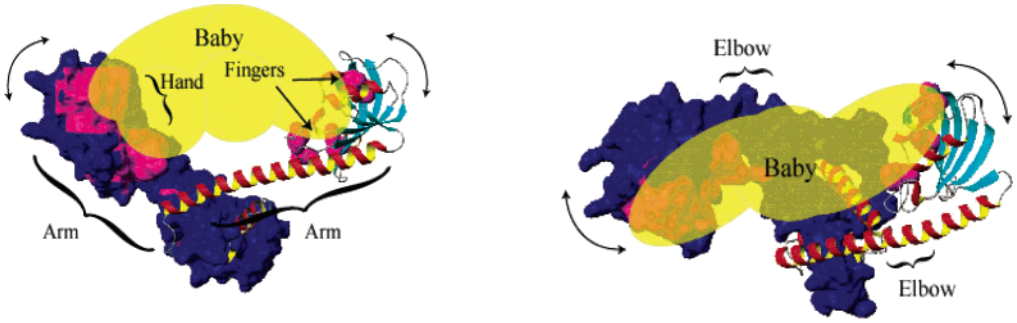

FIGURE 5: The model of "mother's arms", illustrating the mechanism of chaperone function of sFkpA using MOLMOL (*37*). The curved double arrows indicate the flexibility in the long α helix which allows sFkpA to adapt to different substrates. In the two orthogonal views, the chaperone-activity related binding interface of the sFkpA dimer is shown in magenta on the left monomer and residues showing chemical shift perturbation upon addition of both RNase A S-protein and RCM-la are highlighted in magenta on the right monomer. The *β* strands, present in the C-terminal domains are shown in light blue, and helical regions are colored red and yellow.

and unlabeled sFkpA. The ^{1}H-^{15}N-correlation spectra of S-protein measured at different protein concentrations and temperature exhibit significant resonance line-broadening and show features of partial unfolding already at room temperature (also observed by CD, fluorescence (*24*), and DSC (*25*) techniques). Around 20 amide moieties situated in structured regions of S-protein exhibit more than one cross-peak per amide moiety with a small difference in chemical shift between the two resonances. This heterogeneous appearance of spectra is attributed to a slow (on the NMR chemical shift time scale) exchange between monomeric and different associated oligomeric states of S-protein in solution with the dimeric form of S-protein likely contributing the most to the intensity of the resonances attributed to oligomeric forms. A majority of the observed backbone resonances of ^{13}C, ^{15}N-labeled S-protein were assigned using a set of triple resonance NMR spectra (manuscript in preparation). Upon dilution of S-protein, a gradual decrease of cross-peak intensities corresponding to the oligomeric states of S-protein is observed in proportion to the decrease of protein concentration (Figure S.3, Supporting Information). This effect can be quantitatively described by a two-site dimerization reaction with a dimerization constant K_d of approximately 2 (±1) mM^{-1} (data not shown).

In the presence of sFkpA, a 3- to 4-fold decrease of relative intensities of cross-peaks stemming from oligomeric species of S-protein is observed (Figure 2), which is equivalent to ca. 10-fold dilution of S-protein. A hypothesis that binding of S-protein by sFkpA simply sequesters S-protein from solution resulting in an effective decrease of its concentration

does not hold, since the remaining intensities of all cross-peaks of S-protein do not proportionally decrease with the increasing chaperone concentration. A more plausible explanation of this experimental observation can be derived from the analysis of oligomerization of RNase A, RNase S, and S-proteins.

The oligomerization of S-protein is a rather complicated process likely including swapping of C-terminal residues between interacting monomers, which has been observed for the native RNase A upon concentration under destabilizing conditions (*26*, *27*) and recently also for RNase S (RNase A S-protein in presence of its cleaved S-peptide) (*28*). RNase A domain-swapped dimers are shown to resemble the basic building blocks of amyloid fibrils, which could also be formed using RNase A when the swapping domain is expanded by insertion of a poly-Gln segment (*42*, *29*). The formation of higher order oligomers (tri-, tetra-, and pentamers) by 3D-domain swapping has also been observed for this protein (*30*), and it is believed that such oligomers may represent nucleation sites in the process of amyloid formation. We attribute the strong decrease of relative peak intensity corresponding to the oligomeric species upon addition of sFkpA to selective binding of the latter to oligomeric species of S-protein. In the chaperone complex, cross-peaks stemming from oligomers of S-protein are not easily detectable due to fast transverse relaxation induced by slow tumbling of the large molecular weight complex. For example, in the case of sFkpA alone, an extensive deuteration of the aliphatic positions is essential to observe cross-peaks in TROSY experiment. S-protein lacking deutaration is unlikely to exhibit strong cross-peaks even in TROSY experiment if it is bound to sFkpA.

Another explanation for the decrease of the cross-peak intensity stemming from oligomers is that sFkpA affects the monomer−dimer equilibrium of S-protein by interacting with an intermediate on the dimerization pathway. Domain-swapped dimers of S-protein were reported to form through isomerization of the *cis* $Asn^{113}-Pro^{114}$ peptide bond in the C-terminal hinge-loop, which becomes *trans* in the dimer (*28*). sFkpA might promote this isomerization step by its PPIase activity, while showing preferential binding affinity to the dimer S-protein, thus, shifting the equilibrium toward the monomeric species. Higher binding affinity to either *trans* or *cis* isomer of the substrate has been previously reported for other PPIases, for example, for cyclophilin A (CypA). MD simulations of the CypA/CA^N complex hinted that the *trans* form might be preferred in the complex (*39*, *40*), and only the *trans* conformation of $Gly^{89}-Pro^{90}$ is found in the CA^N/CypA cocrystal structure. In contrast, $CypA^{R55A}$ is shown to have higher affinity to CA^N *cis* isomer relative to its *trans* counterpart (*38*). Experimentally, we did not observe any perturbations of TROSY cross-peaks assigned to the monomeric species of S-protein. It might indicate that the monomers of S-protein bind to sFkA only weakly and the monomer-to-dimer interconversion rate is not affected by sFkpA. This is different from previously reported catalysis of *cis/trans* isomerization in CA^N protein by CypA (*38*, *41*), in which the catalyzed isomerization is believed to result in a faster exchange between the *cis* and *trans* isomers.

Our titration data imply that a bacterial periplasmic chaperone selectively interacts with the oligomeric form of S-protein with the *trans* form peptidyl−prolyl bond, thus, effectively terminating the potential oligomerization pathway. The finding that the chaperone specifically binds oligomers but not the thermodynamically destabilized monomers gives insights into the mechanism of the chaperone function and specificity.

Intramolecular Dynamics of sFkpA Studied by ^{15}N Relaxation and Residual Dipolar Couplings. The analysis of the secondary structure of sFkpA in solution demonstrated a break in the regular structure in the center region of a long α-helix connecting the dimerization and catalytic domains of the free chaperone (helix III, residues 70−111) (*9*). We argued that this dynamical disorder might endow the protein with a degree of conformational flexibility in order to accommodate protein substrates of variable size. Here, we employ ^{15}N relaxation and RDCs measurements of backbone amide moieties to further characterize the local conformational restrictions in the protein sequence as well as dynamics of global relative orientation of the protein domains. Both of these types of intramolecular dynamics are likely to have implications for the chaperone function of FkpA.

Figure 3A,C shows the overall pattern of variations in the ^{15}N R_1 and R_2 rates as a function of residue number. Two distinct regions of free FkpA (residues 30−85 and 95−220) with different dynamic properties linked by a rather flexible hinge region (residues 87−94) can be identified. A step-like change in the trend line of the ^{15}N R_1 rates with the average R_1 rates of 0.45 and 0.62 s^{-1} corresponding to the N-terminal dimerization and C-terminal catalytic domain, respectively, is observed (Figure 3A). As low NOE values usually indicate an increased local mobility, it can be concluded that some residues in the long α-helix (e.g., Lys 85, Ala 90, Met 92, and Glu 93) exhibiting low NOE values (smaller that 0.5) are more mobile than the rest of the helix III. The different relaxation properties of N-terminal and C-terminal domains, indicating an intramolecular mobility of the entire C-terminal catalytic domains relative to the N-terminal dimerization domains, might be caused by increased flexibility within the long helix III. The very dispersive pattern of the ^{15}N R_2 rates may suggest the presence of conformational exchange-induced ^{15}N line broadening in the free form of sFkpA.

The S-protein loaded sFkpA exhibits significantly smaller difference in the characteristic ^{15}N R_1 rates of N- and C-terminal domains (Figure 3B) accompanied by a more uniform profile of the ^{15}N R_2 rates of the residues situated in the catalytic domain (Figure 3D). Both of these observations indicated decreased intradomain as well as interdomain flexibility of the substrate-loaded chaperone molecule. Interestingly, that the residues 87−94 situated in the center of the long helix III remain mobile in the complex as well as in the free form of sFkpA. The presence of interdomain as well as intradomain conformational dynamics covering the picosecond to millisecond time scales precluded us from the use of the standard model-free interpretation of the ^{15}N relaxation rates. Additional relaxation data measured at different spectrometer fields would be required for a successful quantitative analysis, which we delegate to the future work. We believe that the qualitative interpretation presented here still suffices for an understanding of the overall dynamic properties of sFkpA relevant to its substrate interactions.

Residual dipolar couplings (RDCs) represent a valuable source of long-range angular information for solution−

Table 1: Results of Fitting a Unique Alignment Tensor to Different Subsets of the RDC Data Measured for sFkpA Aligned With Pf1 Filamentous Bacteriophage at 37 °C[a]

				alignment tensors			
no.	data	data size	Molecule model	A_{xx}	A_{yy}	A_{zz}	correlation coefficient
1	Ex_loop	117	dimer	−10.53	−14.97	25.50	0.747
2	Ex_loop	117	monomer *l*	−12.73	−19.74	32.47	0.872
3	Ex_loop_Nterm	44	dimer	−11.69	−39.20	50.88	0.684
4	Ex_loop_Nterm	44	monomer *l*	−10.03	−15.36	25.39	0.714
5	Ex_loop_Nterm	44	monomer *r*	−5.12	−16.27	21.39	0.606
6	Ex_loop_Cterm	73	dimer	−8.04	−89.12	97.16	0.766
7	Ex_loop_Cterm	73	monomer *l*	−15.32	−21.93	37.24	0.949
8	Ex_loop_Cterm	73	monomer *r*	−15.20	−21.20	36.41	0.950

[a] Ex_loop is data (Table S.2, Supporting Information) in which RDCs from the flexible part of the protein are excluded. Nterm refers to RDC data from the N-terminal (residues 18−112) data, and Cterm stands for data from C-terminal residues 116−224. A_{xx}, A_{yy}, and A_{zz} are the main axis components of Cartesian alignment tensor in the principal axis system (PAS), with relation $|A_{xx}| \leq |A_{yy}| \leq |A_{zz}|$ and $A_{xx} + A_{yy} + A_{zz} = 0$.

structure determinations of macromolecules by NMR spectroscopy (*31*). RDCs can also be employed to determine the relative orientation of domains and study protein dynamics (*32*−*35*). The results of fitting different subsets of the measured RDCs to the corresponding X-ray crystal structural coordinates (PDB code: 1Q6H) are reported in Table 1. Although it has been established that the effect of nonuniform order parameters of intramolecular motion, S^2, on the calculated alignment tensor is minimal (*33*, *34*), to eliminate potential artifacts, only residues located in secondary structure and with low internal mobility (steady-state ^{1}H-^{15}N NOE greater than 0.6) were considered. Interdomain motions were investigated by comparing the quality of fits of alignment tensors obtained from the relevant RDC data using the following coordinates of the X-ray structure (Table 1): (1) a rigid dimeric scaffold consisting of both monomers, (2) only monomer *l*, (3) N-terminal domain of both monomers, (4) N-terminal domain of monomer *l*, (5) N-terminal domain of monomer *r*, (6) C-terminal domain of both monomers, (7) C-terminal domain of monomer *l*, and (8) C-terminal domain of monomer *r*. The low correlation coefficient of 0.747 obtained for the complete dimer suggests that the average molecular geometry in solution is not adequately represented by the X-ray coordinates of free sFkpA. The same RDCs set is then fit using coordinates containing the structural information only from one subunit arbitrary designated as the monomer *l* or *r* (Table 1, line 2). The resulted correlation coefficient is still pretty low (0.872) which further indicates that interdomain mobility rather than a flexible association of the individual monomers into the dimeric scaffold is responsible for the poor fit. Significantly improved correspondence between experimental and molecular model-derived RDCs is obtained in the cases when experimental RDCs fit separately to the molecular models representing the N-terminal residues 18−112 and the C-terminal residues 116−224. Two C-terminal domains are assumed to be able to move independently relative to each other. In this case, alignment tensor fitting to the experimental data can be calculated using coordinates containing the structural information from only one subunit, monomer *l* or monomer *r*. The calculated results of alignment tensor fitting are shown in Table 1 (lines 7 and 8). The data from the C-terminal residues are also fit with a single unique tensor using "Molecule Model" of "Dimer" (Table 1, No. 6), which gives unsatisfactory correlation coefficient as low as 0.766. This low correlation coefficient suggests that the two C-terminal domains are indeed rather highly independent within the dimeric molecular scaffold. The relatively high correlation coefficients calculated from both monomer *l* and monomer *r* (0.949 and 0.950, respectively) suggest that these two C-terminal domains are quite rigid within each subunit itself. The experimental and calculated RDCs for the C-terminal residues of sFkpA are plotted in Figure 4A−C. Similarly, in no. 3−5 in Table 1, fitting of measured RDCs from the N-terminal residues are carried out using different molecular models. Low correlation coefficient of fitting no. 3 (0.684) suggests that there is intramolecular mobility between (or within) these two N-terminal domains within the dimeric scaffold; that is, the mobility could be intrasubunit or intersubunit motion. Using monomer *l* and *r* as molecular models, respectively, in contrast to what was described above for the two C-terminal domains, fitting nos. 4 and 5 yield low correlation coefficients of 0.714 and 0.606, respectively, which excludes the assumption that the two N-terminal domains are highly independent of each other but rigid within each subunit itself. These results suggest that the average solution structure of the dimerization domain might deviate from that in the X-ray structure.

Fitting of RDCs measured at 25 °C on sFkpA in the presence of $C_{12}E_5$/hexanol/H_2O liquid crystalline phase (Table S.1, Supporting Information) gives very good agreement with the results from fitting of RDCs measured at 37 °C on sFkpA aligned with the Pf1 filamentous bacteriophages (Table S.3, Supporting Information). These data further support the view of sFkpA as consisting of two independently moving juxtaposed C-domains adequately represented in the X-ray structure and a rigid dimerization domain exhibiting in solution an averaged structure deviating from the static crystal structure.

The complexity of the motions experienced by sFkpA is difficult to analyze with simple extensions of the classical Lipari−Szabo approach (*43*) due to coupling between interdomain and global reorientation motions of the multidomain protein (*44*). A similar situation holds for the RDC analysis. More quantitative characterization of the restrictions of ligand-modulated interdomain motions based on NMR data have been recently introduced (*44*, *45*). Shapiro et al. successfully applied slowly relaxing local structure ^{15}N relaxation analysis to define relative orientations of two domains of AKeco, an adenylate kinase from *Escherichia coli* in a free from and in a complex with an inhibitor (*45*). The most close case to sFkpA is an application of molecular dynamics simulations in millisecond time scales in a combination with isotropic Reorientational Eigenmode Dynamics (iRED) to peptidyl−prolyl *cis/trans* isomerase Pin1 consisting of two loosly interacting (in the absence of peptide ligands) functional domains connected by a flexible 12 amino acid linker. NMR analysis established that Pin1 can either behave as two independent domains or as a single intact domain with some amount of hinge bending motion when bound to peptide ligands (*46*). These studies open an interesting possibility to characterize more quantitatively the interdomain motions found in sFkpA, which can be delegated to the future work.

Mother's Arms Model of Chaperone Activity. The backbone ^{15}N-relaxation data and residual dipolar couplings (RDCs) showed significant intramolecular mobility of the C-terminal catalytic domains relative to the dimerization domain (N-terminal domain). This agrees with the previously reported variation in the relative orientation of the two C-terminal domains located at the extremities of the V (*2*). This motion is likely to be mediated by a hinge region in the long helix III located between residues 84 and 91, which corresponds to a structural distortion observed in the helix around residue 91 in the X-ray structure of dimeric FkpA-ΔCT (*2*). Similar distortion of the long α-helix around residue 81 has been reported in the X-ray structure of the structurally related protein LpMip both before and after it binds to an inhibitor FK506 (*36*). Considerable plasticity in the long α-helix may be a key to the chaperone function of FkpA, which renders it able to bind a wide range of targets. To locate the chaperone function-related polypeptide-binding site, sFkpA was titrated with S-protein and reduced-carboxymethylated bovine α-lactalbumin (RCM-la), and chemical shift perturbation of sFkpA was mapped to published X-ray structure of dimeric FkpA-ΔCT. The result reveals that the chaperone function related polypeptide-binding sites are located on the internal sides of the two C-terminal domains at the extremities of the V, roughly forming a face-to-face binding interface. On the basis of the recently published X-ray structure of dimeric FkpA-ΔCT, our NMR data enabled us to propose a so-called "mother's arms" model to illustrate the molecular mechanism of the chaperone activity of sFkpA, as shown in Figure 5. In this model, FkpA has two long flexible "arms" (the two long α helices) which can bend at the "elbows" (presumably between residues 84 and 91 within the long α helices). Two "hands", consisting of "fingers", residues Val 142, Val 143, Asp^- 157, Phe 168/Arg^+ 169, Val 205, and Gly 207, are the polypeptide binding sites located on the two C-terminal domains. These two hands can "catch" (interact with) its polypeptide or small protein (the "baby") substrates. The "mother", the dimeric FkpA, through bending of her two long α-helical "arms", can then hold the "baby" (polypeptide or small protein substrate), which is like a mother's arms hugging around her baby.

ACKNOWLEDGMENT

This work was funded by the Swiss National Foundation and the ETH Zürich. We gratefully acknowledge Dr. Beat Vögeli for stimulating discussions. We are grateful to Prof. Andreas Plückthun for the plasmid containing sFkpA and Dr. Christiane Ritter for providing ^{15}N-labeled S-protein samples.

SUPPORTING INFORMATION AVAILABLE

Measured RDCs on sFkpA aligned in $C_{12}E_5$/hexanol/H_2O liquid crystalline and with Pf1 filamentous bacteriophages; alignment tensor fitting results from RDCs of sFkpA measured in $C_{12}E_5$/hexanol/H_2O liquid crystalline; chemical shift changes of sFkpA upon addition of RNase A S-protein and RCM-la; chemical shift changes of residues 99, 102, 157, 168, 205, and 207 of sFkpA upon addition of RNase A S-protein at molar ratios of 1:0.5, 1:1, 1:1.6, and 1:2 which are used for fitting to determine residue-specific K_a. TROSY and H-anti-TROSY spectra of sFkpA for measuring RDCs; an overlay of 2D ^{1}H-^{15}N TROSY spectra of sFkpA titrated with RNase A S-protein and RCM-la at different molar ratios; ratio of dimer-to-monomer peak volume for residues Q60, G68, D83, S90, C95, and K98 of S-protein titrated by sFkpA. This material is available free of charge via the Internet at http://pubs.acs.org.

REFERENCES

1. Horne, S. M., and Young, K. D. (1995) *Escherichia coli* and other species of the Enterobacteriaceae encode a protein similar to the family of MIP-like FK506-binding proteins, *Arch. Microbiol. 163*, 357−365.
2. Saul, F. A., Arié, J. P., Normand, B. V. L., Kahn, R., Betton J. M., and Bentley G. A. (2004) Structural and functional studies of FkpA from *Escherichia coli*, a cis/trans peptidyl-prolyl isomerase with chaperone activity, *J. Mol. Biol. 335*, 595−608.
3. Ramm, K., and Plückthun, A. (2000) The periplasmic *Escherichia coli* peptidylprolyl cis, trans-isomerase FkpA. II. Isomerase-independent chaperone activity in vitro, *J. Biol. Chem. 275*, 17106−17113.
4. Ramm, K., and Plückthun, A. (2001) High enzymatic activity and chaperone function are mechanistically related features of the dimeric *E. coli* peptidyl-prolyl-isomerase FkpA, *J. Mol. Biol. 310*, 485−498.
5. Arié, J. P., Sassoon, N., and Betton, J. M. (2001) Chaperone function of FkpA, a heat shock prolyl isomerase, in the periplasm of *Escherichia coli*, *Mol. Microbiol. 39*, 199−210.
6. Bothmann, H., and Plückthun, A. (2000) The periplasmic *Escherichia coli* peptidylprolyl cis, trans-isomerase FkpA. I. Increased functional expression of antibody fragments with and without cis-prolines, *J. Biol. Chem. 275*, 17100−17105.
7. Scholz, C., Schaarschmidt, P., Engel, A. M., Andres, H., Schmitt, U., Faatz, E., Balbach, J., and Schmid, F. X. (2005) Functional solubilization of aggregation-prone HIV envelope proteins by covalent fusion with chaperone modules, *J. Mol. Biol. 345*, 1229−1241.
8. Padiolleau-Lefevre, S., Debat, H., Phichith, D., Thomas, D., Friboulet, A., and Avalle, B. (2006) Expression of a functional scFv fragment of an anti-idiotypic antibody with a beta-lactam hydrolytic activity, *Immunol. Lett. 103*, 39−44.
9. Hu, K., Plückthun, A., and Pervushin, K. (2004) Letter to the Editor: Backbone H-N, N, C-alpha, C′ and C-beta chemical shift assignments and secondary structure of FkpA, a 245-residue peptidyl-prolyl cis/trans isomerase with chaperone activity, *J. Biomol. NMR 28*, 405−406.
10. Ruckert, M., and Otting, G. (2000) Alignment of biological macromolecules in novel nonionic liquid crystalline media for NMR experiments, *J. Am. Chem. Soc. 122*, 7793−7797.
11. Bartels, C., Xia, T. H., Billeter, M., Guntert, P., and Wuthrich, K. (1995) The program Xeasy for computer-supported NMR spectral-analysis of biological macromolecules, *J. Biomol. NMR 6*, 1−10.
12. Keller, R. L. J. (2004) *The Computer Aided Resonance Assignment Tutorial*, 1st ed., Cantina Verlag, Germany.
13. Wishart, D. S., Bigam, C. G., Yao, J., Abildgaard, F., Dyson, H. J., Oldfield, E., Markley, J. L., and Sykes, B. D. (1995) H-1, C-13 and N-15 chemical-shift referencing in biomolecular NMR, *J. Biomol. NMR 6*, 135−140.
14. Farrow, N. A., Muhandiram, R., Singer, A. U., Pascal, S. M., Kay, C. M., Gish, G., Shoelson, S. E., Pawson, T., Forman-Kay, J. D., and Kay, L. E. (1994) Backbone dynamics of a free and a phosphopeptide-complexed Src homology-2 domain studied by N-15 NMR relaxation, *Biochemistry 33*, 5984−6003.
15. Hansen, M. R., Mueller, L., and Pardi, A. (1998) Tunable alignment of macromolecules by filamentous phage yields dipolar coupling interactions, *Nat. Struct. Biol. 5*, 1065−1074.
16. Lee, D., Vögeli, B., and Pervushin, K. (2005) Detection of C', C^α correlations in proteins using a new time- and sensitivity-optimal experiment, *J. Biomol. NMR 31*, 273−278.
17. Richards, F. M., and Wyckow, H. W. (1971) Bovine pancreatic ribonucleases, in *The Enzymes* (Boyer, P. D., Ed.) pp 647-806, Academic Press, New York.
18. Ritter, C., and Helenius, A. (2000) Recognition of local glycoprotein misfolding by the ER folding sensor UDP-glucose: glycoprotein glucosyltransferase, *Nat. Struct. Biol. 7*, 278−280.
19. Kim, E. E., Varadarajan, R., Wyckoff, H. W., and Richards, F. M. (1992) Refinement of the crystal-structure of ribonuclease-S.

Comparison with and between the various ribonuclease-A structures, *Biochemistry 31*, 12304−12314.
20. True, H. L. (2006) The battle of the fold: chaperones take on prions, *Trends Genet. 22*, 110−117.
21. Hohfeld, J., Cyr, D. M., and Patterson, C. (2001) From the cradle to the grave: molecular chaperones that may choose between folding and degradation, *EMBO Rep. 2*, 885−890.
22. Damberg, C. S., Orekhov, V. Y., and Billeter, M. (2002) Automated analysis of large sets of heteronuclear correlation spectra in NMR-based drug discovery, *J. Med. Chem. 45*, 5649−5654.
23. Petros, A. M., Ramesh, V., and Llinas, M. (1989) H-1-NMR studies of aliphatic ligand-binding to human-plasminogen Kringle-4, *Biochemistry 28*, 1368−1376.
24. Labhardt, A. M. (1984) Kinetic circular dichroism shows that the S-peptide alpha-helix of ribonuclease S unfolds fast and refolds slowly, *Proc. Natl. Acad. Sci. U.S.A. 81*, 7674−7678.
25. Stelea, S. D., Pancoska, P., Benight, A. S., and Keiderling, T. A. (2001) Thermal unfolding of ribonuclease A in phosphate at neutral pH: deviations from the two-state model, *Protein Sci. 10*, 970−978.
26. Liu, Y., Hart, P. J., Schlunegger, M. P., and Eisenberg, D. (1998) The crystal structure of a 3D domain-swapped dimer of RNase A at a 2.1-Å resolution, *Proc. Natl. Acad. Sci. U.S.A. 95*, 3437−3442.
27. Crestfield, A. M., Stein, W. H., and Moore, S. (1962) On the aggregation of bovine pancreatic ribonuclease, *Arch. Biochem. Biophys. Suppl. 1*, 217−222.
28. Lopez-Alonso, J. P., Bruix, M., Font, J., Ribo, M., Vilanova, M., Rico, M., Gotte, G., Libonati, M., Gonzalez, C., and Laurents, D. V. (2006) Formation, structure and dissociation of the ribonuclease S three-dimensional domain-swapped dimer, *J. Biol. Chem. 281*, 9400−9406.
29. Liu, Y., Gotte, G., Libonati, M., and Eisenberg, D. (2001) A domain-swapped RNase A dimer with implications for amyloid formation, *Nat. Struct. Biol. 8*, 282−284.
30. Liu, Y., Gotte, G., Libonati, M., and Eisenberg, D. (2002) Structures of the two 3D domain-swapped RNase A trimers, *Protein Sci. 11*, 371−380.
31. Prestegard, J. H., Tolman, J. R., Al-Hashimi, H. M., and Andrec, M. (1999) Structure computation and dynamics in protein NMR, in *Biological Magnetic Resonance*, (Krishna, N. R., and Berliner, L. J., Eds.) Vol 17, pp 314−320, Kluwer Academic/Plenum Publishers, New York.
32. Tolman, J. R., Al-Hashimi, H. M., Kay, L., and Prestegard, J. H. (2001) Structural and dynamic analysis of residual dipolar coupling data for proteins, *J. Am. Chem. Soc. 123*, 1416−1424.
33. Clore, G. M., and Schwieters, C. D. (2004) How much backbone motion in ubiquitin is required to account for dipolar coupling data measured in multiple alignment media as assessed by independent cross-validation? *J. Am. Chem. Soc. 126*, 2923−2938.
34. Vögeli, B., Kovacs, H., and Pervushin, K. (2004) Measurements of side-chain C-13-C-13 residual dipolar couplings in uniformly deuterated proteins, *J. Am. Chem. Soc. 126*, 2414−2420.
35. Bernado, P., and Blackledge, M. (2004) Anisotropic small amplitude peptide plane dynamics in proteins from residual dipolar couplings, *J. Am. Chem. Soc. 126*, 4907−4920.
36. Riboldi-Tunnicliffe, A., Konig, B., Jessen, S., Weiss, M. S., Rahfeld, J., Hacker, J., Fischer, G., and Hilgenfeld, R. (2001) Crystal structure of MIP, a prolylisomerase from *Legionella pneumophila*, *Nat. Struct. Biol. 8*, 779−783.
37. Koradi, R., Billeter, M., and Wuthrich, K. (1996) MOLMOL: a program for display and analysis of macromolecular structures, *J. Mol. Graphics 14*, 51−55, 29−32.
38. Bosco, D. A., Eisenmesser, E. Z., and Pochapsky, S. (2002) Catalysis of cis/trans isomerization in native HIV-1 capsid by human cyclophilin A, *Proc. Natl. Acad. Sci. U.S.A. 99*, 5247−5252.
39. Agarwal, P. K. (2004) Cis/trans isomerization in HIV-1 capsid protein catalyzed by cyclophilin A: Insights from computational and theoretical studies, *Proteins 56*, 449−463.
40. Agarwal, P. K., Geist, A., and Gorin, A. (2004) Protein dynamics and enzymatic catalysis: Investigating the peptidyl−prolyl cis−trans isomerization activity of cyclophilin A, *Biochemistry 43*, 10605−10618.
41. Eisenmesser, E. Z., Bosco, D. A., Akke, M., and Kern, D. (2002) Enzyme dynamics during catalysis, *Science 295*, 1520−1523.
42. Sambashivan, S., Liu, Y. S., and Sawaya, M. R. (2005) Amyloid-like fibrils of ribonuclease A with three-dimensional domain-swapped and native-like structure, *Nature 437*, 266−269.
43. Lipari, G., and Szabo, A. (1982) Model-free approach to the interpretation of nuclear magnetic-resonance relaxation in macromolecules. 1. Theory and range of validity, *J. Am. Chem. Soc. 104*, 4546−4559.
44. Bernado, P., Fernandes, M. X., and Jacobs, D. M. (2004) Interpretation of NMR relaxation properties of Pin1, a two-domain protein, based on Brownian dynamic simulations, *J. Biomol. NMR 29*, 21−35.
45. Shapiro, Y. E., Kahana, E., and Tugarinov, V. (2002) Domain flexibility in ligand-free and inhibitor-bound *Escherichia coli* adenylate kinase based on a mode-coupling analysis of N-15 spin relaxation, *Biochemistry 41*, 6271−6281.
46. Jacobs, D. M., Saxena, K., and Vogtherr, M. (2003) Peptide binding induces large scale changes in inter-domain mobility in human Pin1, *J. Biol. Chem. 278*, 26174−26182.

BI0607913